Mechanical stability of possible structures of PtN investigated using first-principles calculations

S. K. R. Patil,[1] S. V. Khare,[2,*] B. R. Tuttle,[3] J. K. Bording,[4] and S. Kodambaka[5]
[1]*Department of Mechanical Engineering, The University of Toledo, Toledo, Ohio 43606, USA*
[2]*Department of Physics and Astronomy, The University of Toledo, Toledo, Ohio 43606, USA*
[3]*School of Science, Behrend College, Penn State University at Erie, Pennsylvania 16513, USA*
[4]*Center for Functional Nanomaterials, Brookhaven National Lab, Upton, New York 11973, USA*
[5]*IBM Research Division, T.J. Watson Research Center, Yorktown Heights, New York 10598, USA*
(Received 11 July 2005; revised manuscript received 30 January 2006; published 30 March 2006)

We report an *ab initio* study of the mechanical stability of platinum nitride (PtN), in four different crystal structures, the rock salt (rs-PtN), zinc-blende (zb-PtN), cooperite, and a face-centered orthorhombic phase. Of these phases only the rs-PtN phase is found to be stable and has the highest bulk modulus $B=284$ GPa. Its electronic density of states shows no band gap making it metallic. The zb-PtN phase does not stabilize or harden by the nitrogen vacancies investigated in this study. Therefore, the experimental observation of super hardness in PtN remains a puzzle.

DOI: 10.1103/PhysRevB.73.104118 PACS number(s): 62.20.Dc, 71.15.Nc, 71.20.−b, 81.05.Je

I. INTRODUCTION

Metal and semiconductor nitrides are an important class of materials having properties of fundamental interest as well as those used in a variety of applications.[1–4] Despite the wide interest in making ever better nitrides for applications, the noble metal nitrides have evaded discovery until the recent synthesis of gold[5] and platinum nitrides. In 2004, Gregoryanz *et al.*[6] reported the synthesis of platinum nitride, PtN. This compound was formed using laser-heated diamond anvil-cell techniques at pressures greater than 45 GPa and temperatures exceeding 2000 K. The compound was then recovered completely at room temperature and pressure and analyzed by electron microprobe techniques. Compositional profiles showed that the Pt to N ratio was close to 1:1 with a little variation given by the formula PtN_{1-x} where $x<0.05$. The synchrotron x-ray diffraction experiment revealed PtN to be face-centered cubic but was unable to distinguish between zinc-blende (zb-PtN) and rocksalt (rs-PtN) structures due to a much stronger Pt signal caused by the large difference between masses of Pt and N. But PtN had a first-order Raman spectrum and hence rocksalt structure was ruled out.[6] As the two first-order bands obtained[6] seemed to correspond to Raman active peaks of a zinc-blende structure, the PtN synthesized was concluded to be of this form. The bulk modulus (B) of this zinc-blende PtN was determined to be 372 ± 5 GPa. This B is comparable to 382 GPa of super hard cubic zinc-blende structure BN.[7] Thus PtN with a zinc-blende structure is the first noble metal nitride experimentally identified to be a super hard material. However, theoretical calculations fail to confirm the high bulk modulus extracted from experiment.

Recent theoretical investigations[8–10] have applied different density functional methods to calculate the lattice constants and bulk moduli of various forms of PtN. These studies conclude that the structure and bulk modulus of the zb-PtN are not consistent with experiments. It is suggested by Yu and Zhang[9] that fluorite structured PtN_2 may explain the experimental observations (see Sec. VIII).

These explorations motivated us to study theoretically different crystal structures of PtN as possible candidates for super hardness. We restricted our study to compounds with 1:1 stoichiometric ratio of Pt:N (except for PtN_2, cf. Sec. VIII). Two of these, the zb- and rs-PtN phases were motivated by results of x-ray measurements.[6] The zb-PtN is found to be mechanically unstable and transformed to a lower energy face-centered orthorhombic (fco)-PtN phase. Thus fco-PtN was studied as a potential phase for super hard PtN. PtS exists in cooperite phase and hence cooperite PtN (co-PtN) was also studied as a possible phase for super hard PtN. The main results of our investigations are as follows. The zb-PtN is found to have a lattice constant close to experiment; however, it is also found to be mechanically unstable and transformed to a lower energy fco-PtN. The bulk modulus of zb-PtN is found from two different methods to be almost half the experimentally derived value consistent with the value reported in Ref. 9. The rs-PtN phase is found to be mechanically stable, i.e., its elastic constants obey the conditions $(C_{11}-C_{12})>0$, $(C_{11}+2C_{12})>0$, $C_{11}>0$, and $C_{44}>0$. It has the highest bulk modulus ($B=284$ GPa) greater than the value of 230 GPa for the zb-PtN phase. This lower value of B in the zb-PtN phase [compared to the experimental value of 372 GPa (Ref. 6)] and also its instability led us to investigate the effect of N vacancies on these properties. We found that for nitrogen vacancy concentrations of 3.7 and 12.5 % that bracketed the value of the maximum 5% reported in experiment, the zb-PtN phase remained unstable and its B hardly changed. Our study indicates that further experimental investigation needs to be carried out to find the cause of the stability and high B of the zb-PtN.

The rest of the paper is organized as follows. Section II gives the details of the *ab initio* method used. Section III describes the structure of four different phases of PtN studied. Section IV illustrates the method of calculation of elastic constants. In Sec. V we investigate the stability of the four phases. Section VI reports the band structure and density of states of rs-PtN. Section VII gives results involving introduction of N vacancies. Section VIII discusses the possibility of

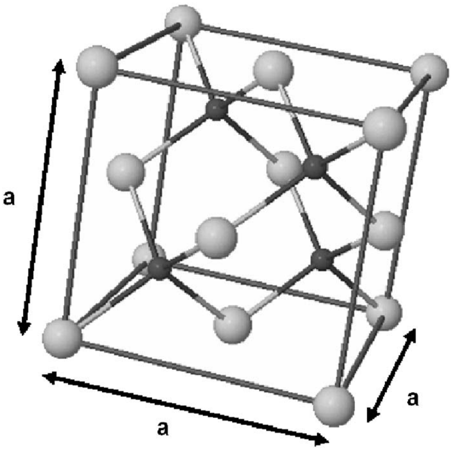

FIG. 1. Zinc-blende structure of PtN. Larger (smaller) atoms are Pt (N). Only nearest neighbor bonds are shown. The lattice constant *a* is given in Table I.

synthesized PtN being a fluorite phase instead of zinc blende as claimed in the experiment.

II. *AB INITIO* METHOD

We performed first-principles total energy calculations within the local density approximation (LDA) and also generalized gradient approximation (GGA) to the density functional theory[11] (DFT) using the suit of codes VASP.[12–15] Core electrons are implicitly treated by ultra soft Vanderbilt-type pseudopotentials[16] as supplied by Kresse and Hafner.[17] For each calculation, irreducible k points are generated according to the Monkhorst-Pack scheme.[18] Convergence is achieved with 408 k points in the irreducible part of Brillouin zone for zb-PtN and rs-PtN structures and with 512 and 864 k points for cooperite and orthorhombic structures, respectively. The single-particle wave functions have been expanded in a plane-wave basis using a 224 eV kinetic energy cutoff. All atoms are allowed to relax until a force tolerance of 0.03 eV/Å is reached for each atom. Tests using a higher plane-wave cutoff and a larger k-point sampling indicate that a numerical convergence better than ±1.0 meV is achieved for relative energies.

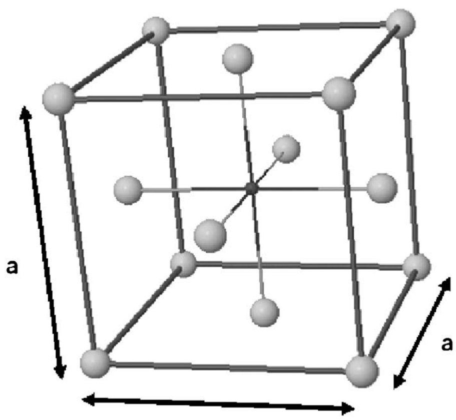

FIG. 2. Rocksalt structure of PtN. Larger (smaller) atom is Pt (N). Only nearest neighbor bonds are shown. The N atoms at the center of each edge of the cube are not shown for clarity. The lattice constant *a* is given in Table I.

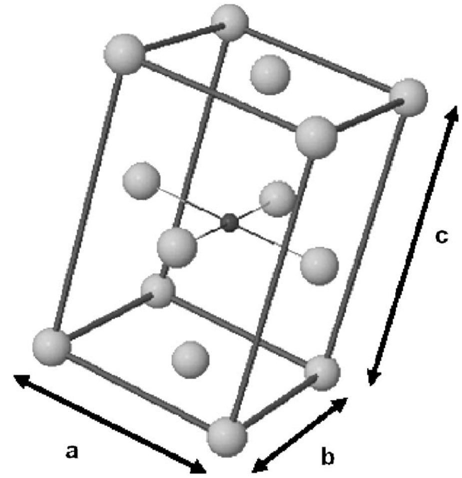

FIG. 3. Face-centered orthorhombic structure of PtN. Larger (smaller) atom is Pt (N). Only nearest neighbor bonds are shown. The N atoms at the center of each edge of the cube are not shown for clarity. The lattice constants *a*, *b*, and *c* are given in Table I.

III. CRYSTAL STRUCTURE

We investigated four different phases of PtN, the (i) zb-PtN structure (space group $F\bar{4}3m$),[19] (ii) rs-PtN structure (space group $Fm\bar{3}m$),[19] (iii) face-centered orthorhombic structure (fco) (space group $Fddd$),[19] and (iv) cooperite (PtS) structure (space group $P4_2/mmc$).[19] The unit cells for the first three phases are shown in Figs. 1–3, respectively. They consist of three lattice constants of the conventional unit cell a, b, and c with lattice vectors $\mathbf{a}_1=\frac{1}{2}\,(0,b,c)$, $\mathbf{a}_2=\frac{1}{2}\,(a,0,c)$, and $\mathbf{a}_3=\frac{1}{2}\,(a,b,0)$. The basis consists of a Pt atom at (0, 0, 0)

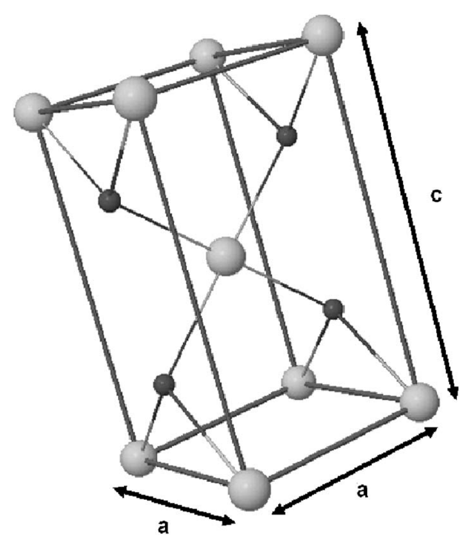

FIG. 4. Tetragonal structure of PtN. Larger (smaller) atom is Pt (N). Only nearest neighbor bonds are shown. The lattice constants *a*, *c* are given in Table I.

TABLE I. Bulk moduli (B) and lattice constants (a,b,c) of different phases of PtN obtained within the local density approximation (LDA) and the generalized gradient approximation (GGA). Two different *ab initio* methods were used in our work for zb-PtN and rs-PtN: (i) VASP (Refs. 13–15), which uses a pseudopotential approach with plane wave basis and (ii) WIEN2K, which is an all electron FLAPW technique. Values from Refs. 8 and 9 are also computed using WIEN2K. The comparison shows that the bulk moduli calculated in the present work (VASP and WIEN2K) are in good agreement with Refs. 8 and 9. Several forms of DFT have been used to obtain B in Ref. 10. Of these methods LSDA most closely resembles our calculations and hence we report the LSDA values. $E_{\text{f-r-t}}$ is the formation energy per PtN formula unit with respect to the tetragonal structure. Bulk modulus for tetragonal PtN is not reported as the involved elastic constants were found to be negative and unstable.

	Present work				Ref. 10	Ref. 9		Ref. 8
	LDA		GGA			LDA	GGA	GGA
Lattice structure	VASP	WIEN2K	VASP	WIEN2K	LSDA	WIEN2K	WIEN2K	WIEN2K
zb-PtN								
Bulk modulus (GPa)	230	235	192	178	231	244	194	185.5
Lattice constant (nm)	0.4699	0.4683	0.4794	0.4781	0.4711	0.4692	0.4780	0.4804
$E_{\text{f-r-t}}$ (eV)	0.42							
rs-PtN								
Bulk modulus (GPa)	284	298	226	233				215.5
Lattice constant (nm)	0.4407	0.4397	0.4504	0.4496				0.4518
$E_{\text{f-r-t}}$ (eV)	0.75							
fco-PtN								
Bulk modulus (GPa)	270							
Lattice constant (nm)	$a=0.3972$							
	$b=0.3977$							
	$c=0.6022$							
$E_{\text{f-r-t}}$ (eV)	0.17							
co-PtN								
Bulk modulus (GPa)								
Lattice constant	$a=0.3323$							
(nm)	$b=a$							
	$c=0.4579$							
$E_{\text{f-r-t}}$ (eV)	0							

and a N atom at $\frac{1}{\alpha}(\mathbf{a}_1+\mathbf{a}_2+\mathbf{a}_3)$. The first two phases have $c=b=a$, giving them a cubic symmetry. The first phase has $\alpha=4$, while the second and third phases have $\alpha=2$. Figure 4 shows the unit cell of co-PtN having lattice constants a and c. The lattice vectors are $\mathbf{a}_1=(a,0,0)$, $\mathbf{a}_2=(0,a,0)$, and $\mathbf{a}_3=(0,0,c)$. Two Pt atoms at (0, 0, 0), $\frac{1}{2}(\mathbf{a}_1+\mathbf{a}_2+\mathbf{a}_3)$ and two N atoms at $\left(\frac{1}{2}\mathbf{a}_2+\frac{1}{4}\mathbf{a}_3\right)$, $\left(\frac{1}{2}\mathbf{a}_2+\frac{3}{4}\mathbf{a}_3\right)$ make up the basis.

The equilibrium lattice constants a, b, and c were varied independently (when they were different) to obtain the absolute minimum in total energy for each structure. All basis atoms were allowed to relax fully. Table I summarizes the equilibrium lattice constants of the different PtN structures. The structure with the lowest total energy per formula unit of PtN was co-PtN. Hence the formation energies $E_{\text{f-r-t}}$ of the other phases are reported with respect to this tetragonal structure in Table I.

IV. ELASTIC CONSTANTS

Elastic constants are the measure of the resistance of a crystal to an externally applied stress. For small strains Hooke's law is valid and the crystal energy E is a quadratic function of strain.[20] Thus, to obtain the total minimum energy for calculating the elastic constants to second order, a crystal is strained and all the internal parameters relaxed. Consider a symmetric 3×3 nonrotating strain tensor $\boldsymbol{\varepsilon}$ which has matrix elements ε_{ij} ($i,j=1$, 2, and 3) defined by Eq. (1)

$$\varepsilon_{ij}=\begin{pmatrix} e_1 & \frac{e_6}{2} & \frac{e_5}{2} \\ \frac{e_6}{2} & e_2 & \frac{e_4}{2} \\ \frac{e_5}{2} & \frac{e_4}{2} & e_3 \end{pmatrix}. \quad (1)$$

Such a strain transforms the three lattice vectors defining the unstrained Bravais lattice $\{\mathbf{a}_{\text{k}}$, k=1, 2, and 3$\}$ to the strained vectors[21] $\{\mathbf{a}'_{\text{k}}$, k=1, 2, and 3$\}$ as given by Eq. (2)

TABLE II. Three strain combinations in the strain tensor [Eq. (1)] for calculating the three elastic constants of cubic structures shown in Figs. 1 and 2. The three independent elastic constants C_{11}, C_{12}, and C_{44} of zinc blende and rock salt PtN are calculated from the above strains. Symmetry dictates $C_{ij}=C_{ji}$ and all unlisted $C_{ij}=0$. The strain δ is varied in steps of 0.01 from $\delta=-0.02$ to 0.02. ΔE [Eq. (3)] is the difference in energy between that of the strained lattice and the unstrained lattice. The equilibrium or unstrained lattice volume is V_0.

Strain	Parameters (unlisted $e_i=0$)	$\Delta E/V_0$
1	$e_1=e_2=\delta$, $e_3=(1+\delta)^{-2}-1$	$3(C_{11}-C_{12})\delta^2$
2	$e_1=e_2=e_3=\delta$	$\frac{3}{2}(C_{11}+2C_{12})\delta^2$
3	$e_6=\delta$, $e_3=\delta^2(4-\delta^2)^{-1}$	$\frac{1}{2}C_{44}\delta^2$

$$\mathbf{a}'_\mathbf{k} = (\mathbf{I} + \boldsymbol{\varepsilon})\mathbf{a}_\mathbf{k}, \tag{2}$$

where $\mathbf{I}$ is defined by its elements, $I_{ij}=1$ for $i=j$ and 0 for $i\neq j$. Each lattice vector $\mathbf{a}_\text{k}$ or $\mathbf{a}'_\text{k}$ is a 3×1 matrix. The change in total energy due to above strain (1) is

$$\frac{\Delta E}{V_0} \equiv \frac{E(\{e_i\}) - E_0}{V_0} = \left(1 - \frac{V}{V_0}\right)P(V_0) + \frac{1}{2}\left(\sum_{i=1}^{6}\sum_{j=1}^{6} C_{ij}e_ie_j\right) + O(\{e_i^3\}), \tag{3}$$

where V_0 is the volume of the unstrained lattice, E_0 is the total minimum energy at this unstrained volume of the crystal, $P(V_0)$ is the pressure of the unstrained lattice, and V is the new volume of the lattice due to strain in Eq. (1). In Eq. (3), $C_{ij}=C_{ji}$ due to crystal symmetry.[20] This reduces the elastic stiffness constants C_{ij}, from 36 to 21 independent elastic constants in Eq. (3). Further crystal symmetry[20,21] reduces the number to 9 (C_{11}, C_{12}, C_{13}, C_{23}, C_{22}, C_{33}, C_{44}, C_{55}, C_{66}) for orthorhombic crystals, 6 (C_{11}, C_{12}, C_{13}, C_{33}, C_{44}, C_{66}) for tetragonal crystals, and 3 (C_{11}, C_{12}, C_{44}) for cubic crystals. A proper choice of the set of strains $\{e_i, i=1,2,\ldots,6\}$, in Eq. (3) leads to a parabolic relationship between $\Delta E/V_0$ ($\Delta E \equiv E-E_0$) and the chosen strain. Such choices for the set $\{e_i\}$ and the corresponding form for ΔE are shown in Table II (Ref. 22) for cubic, Table III (Ref. 23) for tetragonal, and Table IV (Ref. 24) for orthorhombic lattices. For each lattice structure of PtN studied, we strained the lattice by 0%, ±1%, and ±2% to obtain the total minimum energies $E(V)$ at these strains. These energies and strains were fit with the corresponding parabolic equations of $\Delta E/V_0$ as given in Tables II–IV to yield the required second-order elastic constants. While computing these energies all atoms are allowed to relax with the cell shape and volume fixed by the choice of strains $\{e_i\}$.

V. MECHANICAL STABILITY

The strain energy $\left(\frac{1}{2}C_{ij}e_ie_j\right)$ of a given crystal in Eq. (3) must always be positive for all possible values of the set $\{e_i\}$; otherwise the crystal would be mechanically unstable. This means that the quadratic form $\left(\frac{1}{2}C_{ij}e_ie_j\right)$ must be positive definite for all real values of strains unless all the strains are zero. This imposes further restrictions on the elastic constants C_{ij} depending on the crystal structure. These stability

TABLE III. Six strain combinations in the strain tensor [Eq. (1)] for calculating the six elastic constants of the tetragonal structure shown in Fig. 3. The six independent elastic constants C_{11}, C_{12}, C_{13}, C_{33}, C_{44}, and C_{66} of tetragonal PtN are calculated from the above strains. Symmetry dictates $C_{ij}=C_{ji}$ and all unlisted $C_{ij}=0$. The strain δ is varied in steps of 0.01 from $\delta=-0.02$ to 0.02. ΔE [Eq. (3)] is the difference in energy between that of the strained lattice and the unstrained lattice. The equilibrium or unstrained lattice volume is V_0.

Strain	Parameters (unlisted $e_i=0$)	$\Delta E/V_0$
1	$e_1=\delta$	$\frac{1}{2}C_{11}\delta^2$
2	$e_3=\delta$	$\frac{1}{2}C_{33}\delta^2$
3	$e_4=2\delta$	$2C_{44}\delta^2$
4	$e_1=2\delta$, $e_2=e_3=-\delta$	$\frac{1}{2}(5C_{11}-4C_{12}-2C_{13}+C_{33})\delta^2$
5	$e_1=e_2=-\delta$, $e_3=2\delta$	$(C_{11}+C_{12}-4C_{13}+2C_{33})\delta^2$
6	$e_1=e_2=\delta$, $e_3=-2\delta$, $e_6=2\delta$	$(C_{11}+C_{12}-4C_{13}+2C_{33}+2C_{66})\delta^2$

TABLE IV. Nine strain combinations in the strain tensor [Eq. (1)] for calculating the nine elastic constants of the orthorhombic structure shown in Fig. 4. The nine independent elastic constants C_{11}, C_{12}, C_{13}, C_{23}, C_{22}, C_{33}, C_{44}, C_{55}, and C_{66} of the orthorhombic PtN are calculated from the above strains. Symmetry dictates $C_{ij}=C_{ji}$ and all unlisted $C_{ij}=0$. The strain δ is varied in steps of 0.01 from $\delta=-0.02$ to 0.02. ΔE [Eq. (3)] is the difference in energy between that of the strained lattice and the unstrained lattice. The equilibrium or unstrained lattice volume is V_0.

Strain	Parameters (unlisted $e_i=0$)	$\Delta E/V_0$
1	$e_1=\delta$	$\frac{1}{2}C_{11}\delta^2$
2	$e_2=\delta$	$\frac{1}{2}C_{22}\delta^2$
3	$e_3=\delta$	$\frac{1}{2}C_{33}\delta^2$
4	$e_4=\delta$	$\frac{1}{2}C_{44}\delta^2$
5	$e_5=\delta$	$\frac{1}{2}C_{55}\delta^2$
6	$e_6=\delta$	$\frac{1}{2}C_{66}\delta^2$
7	$e_1=2\delta,\ e_2=e_3=-\delta$	$\frac{1}{2}(4C_{11}-4C_{12}-4C_{13}+C_{22}+2C_{23}+C_{33})\delta^2$
8	$e_1=-\delta,\ e_2=2\delta,\ e_3=-\delta$	$\frac{1}{2}(C_{11}-4C_{12}+2C_{13}+4C_{22}-4C_{23}+C_{33})\delta^2$
9	$e_1=e_2=-\delta,\ e_3=2\delta$	$\frac{1}{2}(C_{11}+2C_{12}-4C_{13}+C_{22}-4C_{23}+4C_{33})\delta^2$

conditions can be determined by standard algebraic methods.[25]

A. zb-PtN

For cubic crystal structures such as those of zb-PtN or rs-PtN, the necessary conditions for mechanical stability are given by[26]

$$(C_{11}-C_{12})>0,\quad (C_{11}+2C_{12})>0,\quad C_{11}>0,\quad C_{44}>0. \tag{4}$$

The elastic constants are determined by applying the strains listed in Table II. $C_{11}-C_{12}$ is obtained by using the strain combination on the first row of Table II. Table V shows the numerical values of our computation of all the elastic constants of zb-PtN. These values satisfy all the stability conditions of Eq. (4) except the condition that $(C_{11}-C_{12})>0$. Thus we have concluded that the zb-PtN is mechanically unstable which contradicts the experimental data.[6]

We now turn our attention to the strain listed on the second row of Table II which is an isotropic strain and it yields, $B=(C_{11}+2C_{12})/3$. We obtained a B value of 230 GPa, which is lower than the experimentally reported value of 372 GPa by 38%.[6] The fit of these isotropically strained volumes and corresponding total minimum energies to Murnaghan equation of state[27] yielded $B=231$ GPa. Thus our theoretical calculations suggest that the experimentally observed structure is unstable and with a B that is far larger than the theoretically expected value. However, the experiment found that the precise stoichiometry for their PtN sample was given by PtN_{1-x} with $0<x<0.05$. To investigate the effect of N vacancies on the stability of zb-PtN and value of B, we did further calculations which are described in Sec. VII. Based on our results we conclude that N vacancies only soften the

TABLE V. All the independent elastic constants, in Giga Pascal (GPa) of PtN in different forms calculated using LDA. Symmetry dictates $C_{ij}=C_{ji}$ and all unlisted $C_{ij}=0$. An unstable elastic constant in the table represents the case when the applied strain to the unit cell leads to a linear combination of C_{ij} to be negative. Elastic constants represented by C_{ij} instead of a numerical value imply that elastic constant is not an independent one, e.g., the value of elastic constant C_{22} of rocksalt is equal to that of C_{11} already calculated to be 248 GPa. Notice that the condition $(C_{11}-C_{12})>0$ from Eq. (4) is not satisfied for zinc-blende structure making it unstable.

C_{ij} (in GPa)	Zinc blende	Rocksalt	Cooperite	Face-centered orthorhombic
C_{11}	210	355	Unstable	570
C_{22}	C_{11}	C_{11}	C_{11}	254
C_{33}	C_{11}	C_{11}	Unstable	258
C_{44}	14	36	Unstable	Unstable
C_{55}	C_{44}	C_{44}	C_{44}	98
C_{66}	C_{44}	C_{44}	Unstable	98
C_{12}	241	248	Unstable	240
C_{13}	C_{12}	C_{12}	Unstable	240
C_{23}	C_{12}	C_{12}	C_{13}	194

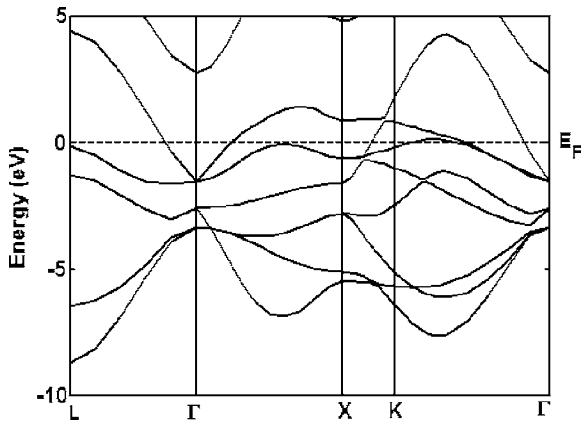

FIG. 5. Band structure of stable rocksalt structure of PtN along high symmetry points calculated using local density approximation (LDA) with Fermi energy level E_F taken at 0 eV as shown by the dotted line. The self-consistent calculations were performed using ultra soft pseudopotentials with the theoretical lattice constant a given in Table I. The symmetry points considered in lattice coordinates are $L(\frac{1}{2},\frac{1}{2},\frac{1}{2})$, X (0, 1, 0), $K(\frac{3}{4},\frac{3}{4},0)$, and Γ (0, 0, 0).

material and do not explain the large experimental value for B (372 GPa).

These disagreements between our theoretically computed properties and the experimental results for zb-PtN motivated us to explore other possible structures of PtN which could potentially yield very large values of the elastic constants and hence super hardness. Since Pt has a large value of $B=298$ GPa (Ref. 28), it would seem plausible to have such an expectation.[6] The x-ray diffraction part of the experimental measurements could not distinguish[6,8] between the zb-PtN and rs-PtN structural types since they both had face-centered cubic (fcc) symmetry. This is because of the much weaker signal of N atoms than that of Pt atoms due to a large difference in their atomic numbers. Also many other monotransition metal nitrides, such as CrN, NbN, VN, and ZrN exist in the NaCl phase. So we explored this phase next.

B. rs-PtN

As rs-PtN is cubic, it has to satisfy all the conditions in Eq. (4) to be mechanically stable. These conditions are indeed satisfied as seen from the calculated elastic constants in Table V, making it mechanically stable. The calculated B with the parabolic fit of strain 2 in Table II was found to be 284 GPa. As zb-PtN is unstable and rs-PtN is stable and because of the fcc structure reported by the x-ray analysis,[6] one would be tempted to conclude that PtN is a rocksalt structure like many other monotransition metal nitrides. But the calculated lattice constant of rocksalt PtN, 0.45036 nm (by GGA) and 0.44071 nm (by LDA) varies substantially from 0.4801 nm measured experimentally.[6] The value of B we obtained was 284 GPa, still off from the experimental value of 372 GPa. It is thus not clear whether the observed PtN is in NaCl structure. We explored the electronic properties of this stable phase (see Sec. VI) because of its stability. With an interest toward finding a super-hard form of PtN we explored two other structures of PtN having 1:1 stoichiometry. The first of these, the tetragonal (cooperite) structure was motivated by the existence in this form of PtO which could exist as a contaminant in the experimental sample.[29]

C. co-PtN

The stability criteria for a tetragonal crystal[26] are

$$(C_{11}-C_{12})>0,\quad (C_{11}+C_{33}-2c_{13})>0,$$

$$(2C_{11}+C_{33}+2C_{12}+4C_{13})>0,$$

$$C_{11}>0,\quad C_{33}>0,\quad C_{44}>0,\quad C_{66}>0. \tag{5}$$

The elastic constants of tetragonal PtN are shown in Table V. The calculated elastic constant C_{44} is negative violating Eq. (5) and so is labeled unstable in Table V. For the strain types 1, 2, 4, 5, and 6 in Table III, the total minimum energy for strained lattice was less than that of the unstrained lattice indicating the transformation of the tetragonal structure to either monoclinic or triclinic structures. Hence, the elastic constants C_{11}, C_{12}, C_{13}, C_{66}, and C_{33} are labeled unstable in Table V, making the tetragonal cell mechanically unstable. Thus the formation of stable PtN in cooperite phase is ruled out. The fourth structure we investigated was discovered by noticing that $C_{11}-C_{12}<0$ in Table V for the zb-PtN. Under the strain corresponding to $C_{11}-C_{12}$ the zinc blende structure transforms to a face-centered orthorhombic (fco) structure.

D. fco-PtN

The mechanical stability criteria for face-centered orthorhombic[24] PtN are

$$(C_{22}+C_{33}-2C_{23})>0,$$

$$(C_{11}+C_{22}+C_{33}+2C_{12}+2C_{13}+2C_{23})>0,$$

$$C_{11}>0,\quad C_{22}>0,\quad C_{33}>0,\quad C_{44}>0,$$

$$C_{55}>0,\quad C_{66}>0. \tag{6}$$

The calculated elastic constants are shown in Table V. All the elastic constants, except for C_{44}, obey the mechanical stability criteria given in Eq. (6). Hence the possibility of PtN crystallizing in face-centered orthorhombic phase is eliminated. For strain-type 4 in Table IV the fco PtN transforms to a triclinic phase, which we did not investigate. We now conclude that of the four forms of PtN we studied rs-PtN is mechanically stable. We describe its electronic structure next.

VI. ELECTRONIC STRUCTURE OF rs-PtN

The band structure of this phase along a high symmetry direction is shown in Fig. 5. The calculated density of states (DOS) is shown in Fig. 6. There is no band gap in the DOS at the fermi level (E_F) and hence rs-PtN is metallic. The bands near the fermi level are mainly contributed by platinum d orbitals while the lowest band is mainly the nitrogen

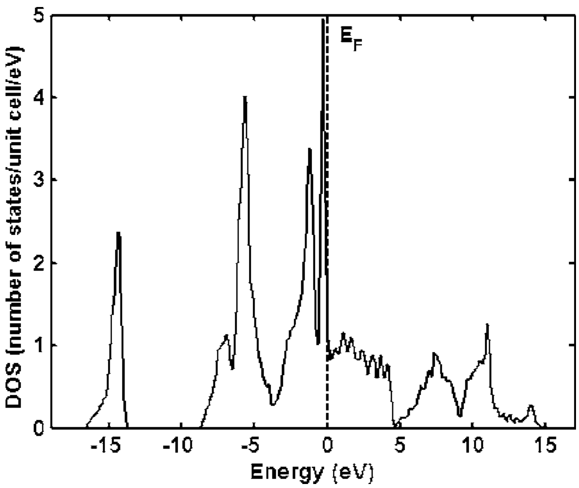

FIG. 6. Density of states (DOS) of stable rocksalt structure of PtN from local density approximation (LDA) calculations with E_F, the Fermi energy level taken at 0 eV as shown by the dotted line. These calculations have been performed at the equilibrium theoretical lattice constant a given in Table I.

s orbital. The electronic density of states is calculated using 408 irreducible k points and a 0.2 eV smearing of the energy levels to provide a smooth DOS plot. The DOS between −5 eV and +1 eV is dominated by the Pt metal states and compares well to the photoemission spectra of platinum.[30] Figure 7 shows the projected density of states (PDOS) of Pt and N atoms in s, p, and d orbitals. As seen from PDOS, the d electrons of Pt contribute to the majority of the DOS near the Fermi level.

VII. NITROGEN VACANCIES

The experimental specimen of PtN_{1-x} was substoichiometric with $0<x<0.05$. This substoichiometry may be the reason for both its stability and high value of B. To check for such a trend, we performed a calculation with a larger supercell[31] to create $Pt_{27}N_{26}$ (i.e., $x=0.0370$) which is comparable to the experimental specimen. The equilibrium lattice constant for this substoichiometric zb-PtN was found to be 0.46019 nm and B was found to be 221 GPa. Thus the bulk modulus is reduced slightly at this nitrogen vacancy concentration. The other substoichiometry computed was a supercell[32] of Pt_8N_7 (i.e., $x=0.125$). The lattice constant and bulk modulus for this compound were 0.45556 nm and 238 GPa, respectively. Thus this composition hardly raises the value of B to the value reported in experiment. The strain-type 1 of Table II for which the zb-PtN was unstable was applied to the above-mentioned two super cells. These calculations showed that the stability criterion $(C_{11}-C_{12})>0$ was not satisfied for these substoichiometric forms. Values of x in our calculations for substoichiometric cases are 0 (no vacancies), 0.037, and 0.125. These values cover the experimental range for x from 0 to 0.05 and beyond. It seems unlikely then that $PtN_{1-x}(0<x<0.05)$, can be stabilized by the presence of vacancies alone. However, stabilizing and hardening effects due to other types of defects or impurities induced by the high pressure and high temperature production technique used in the experiment cannot be ruled out.

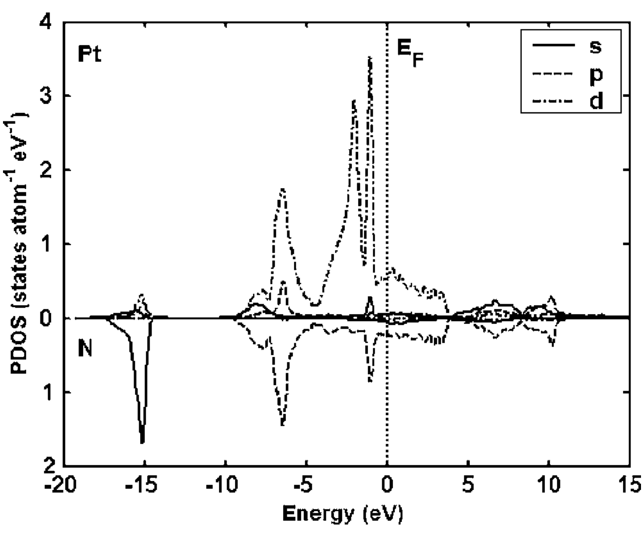

FIG. 7. s, p, and d projected density of states (PDOS) in the Pt and N spheres for stable rocksalt phase of PtN with E_F, the Fermi energy level taken at 0 eV as shown by the dotted line.

VIII. FLUORITE PHASE OF PtN

Yu and Zhang[9] have suggested that the experimental sample may contain excess N atoms, and hence may well be the PtN_2 fluorite phase in the $Fm\bar{3}m$ space group. As a check, we also calculated the bulk modulus and elastic constants of PtN_2 using VASP. The bulk modulus was found to be 300 GPa. The computed elastic constants C_{11}, C_{12}, and C_{44} were 495, 193, and 109 GPa, respectively, satisfying the mechanical stability conditions for cubic lattices as given in Eq. (4). These values for fluorite PtN_2 are in good agreement with those obtained in Ref. 9 [$C_{11}=532$ GPa, $C_{12}=208$ GPa, $C_{44}=122$ GPa].

IX. SUMMARY

Using first-principles calculations we have computed properties of PtN, a recently synthesized noble metal nitride.[6] Using our *ab initio* calculations the experimental zinc-blende structure of PtN reported[6] was found to be mechanically unstable and its bulk modulus was found to be 38% lower than in experiment. Upon introduction of N vacancies in this zb-PtN structure we found that it remained unstable and the bulk modulus did not change substantially. The role of other types of impurities or defects causing the stability and super hardness cannot be ruled out. Further experimental investigation is needed to understand the underlying causes for stability and super hardness, which are not explained by our *ab initio* calculations.

To find super hardness in other forms of PtN we also investigated its rocksalt, cooperite, and face centered orthorhombic phases. Of these only rs-PtN was found to be stable.

X-ray diffraction measurements[6] have identified this form as a possible structural candidate showing fcc symmetry. However, our calculated lattice constant 0.45036 nm differs from the experimental value of 0.48010 nm by 6.2%. We also find no evidence for super hardness in this form. The electronic band structure and total density of states of this stable phase were studied. rs-PtN does not show band gap and is metallic consistent with experimental observation. All our computations and those of others[8–10] reveal that more experiments need to be performed to ascertain the true nature of the newly discovered PtN material.

We recently became aware of C. Z. Fan *et al.* (Ref. 33), who have also discovered the instability of zb-PtN.

ACKNOWLEDGMENTS

This work was partially supported by the Division of Materials Sciences, Office of Basic Energy Science, U.S. Department of Energy. S. V. Khare acknowledges support from the University of Toledo, Office of Research, URAF 2005 award. We thank Ohio Supercomputer Center for providing computing resources.

*Corresponding author. Electronic address: khare@physics.utoledo.edu

[1] M. W. Barsoum, Prog. Solid State Chem. **28**, 201 (2000).
[2] J. S. Chun, I. Petrov, and J. E. Greene, J. Appl. Phys. **86**, 3633 (1999).
[3] A. E. Kaloyeros and E. Eisenbraun, Annu. Rev. Mater. Sci. **30**, 363 (2000).
[4] S. H. Jhi, J. Ihm, S. G. Louie, and M. L. Cohen, Nature (London) **399**, 132 (1999).
[5] S. Krishnamurthy, M. Montalti, M. G. Wardle, M. J. Shaw, P. R. Briddon, K. Svensson, M. R. C. Hunt, and L. Siller, Phys. Rev. B **70**, 045414 (2004).
[6] E. Gregoryanz, C. Sanloup, M. Somayazulu, J. Bardo, G. Fiquet, H.-K. Mao, and R. Hemley, Nat. Mater. **3**, 294 (2004).
[7] E. V. Yakovenko, I. V. Aleksandrov, A. F. Gonchavrov, and S. M. Stishov, Sov. Phys. JETP **68**, 1213 (1989).
[8] B. R. Sahu and L. Kleinman, Phys. Rev. B **71**, 041101(R) (2005); **71**, 209904(E) (2005); **72**, 119901(E) (2005).
[9] R. Yu and X. F. Zhang, Appl. Phys. Lett. **86**, 121913 (2005).
[10] J. Uddin and G. E. Scuseria, Phys. Rev. B **72**, 035101 (2005); **72**, 119902(E) (2005).
[11] P. Hohenberg and W. Kohn, Phys. Rev. **136**, B864 (1964); W. Kohn and L. J. Sham, Phys. Rev. **140**, A1133 (1965).
[12] G. Kresse and J. Hafner, Phys. Rev. B **47**, R558 (1993).
[13] G. Kresse, Thesis, Technische Universiät Wien 1993.
[14] G. Kresse and J. Furthmüller, Comput. Mater. Sci. **6**, 15 (1996).
[15] G. Kresse and J. Furthmüller, Phys. Rev. B **54**, 11169 (1996).
[16] D. Vanderbilt, Phys. Rev. B **41**, R7892 (1990).
[17] G. Kresse and J. Hafner, J. Phys.: Condens. Matter **6**, 8245 (1994).
[18] H. J. Monkhorst and J. D. Pack, Phys. Rev. B **13**, 5188 (1976).
[19] See for different crystal models: http://cst-www.nrl.navy.mil/lattice/prototype.html
[20] J. F. Nye, *Physical Properties of Crystals, Their Representation by Tensors and Matrices* (Oxford Press, 1957), Chap VIII.
[21] *Intermetallic Compounds: Principles and Practice, Vol I: Principles*, edited by J. H. Westbrook and R. L. Fleischer (Wiley, London, 1995), Chap. 9 pp. 195–210.
[22] M. J. Mehl, J. E. Osburn, D. A. Papaconstantopoulos, and B. M. Klein, Phys. Rev. B **41**, 10311 (1990); **42**, 5362(E) (1990).
[23] M. Alouani, R. C. Albers, and M. Methfessel, Phys. Rev. B **43**, 6500 (1991).
[24] O. Beckstein, J. E. Klepeis, G. L. W. Hart, and O. Pankratov, Phys. Rev. B **63**, 134112 (2001).
[25] W. L. Ferrar, *Algebra: A Text-Book of Determinants, Matrices, and Algebraic Forms* (Oxford University Press, Oxford, U.K., 1941), p. 138.
[26] D. C. Wallace, *Thermodynamics of Crystals* (Wiley, New York, 1972), Chap. 1.
[27] F. D. Murnaghan, Proc. Natl. Acad. Sci. U.S.A. **30**, 244 (1944).
[28] J. J. Gilman, *Electronic Basis of the Strength of Materials* (Cambridge University Press, UK, 2003), Chap. 12.
[29] As an example: It is known that TiO is iso-structural with NaCl structure of TiN and that both have similar lattice constants. See S. Kodambaka, S. V. Khare, V. Petrova, D. D. Johnson, I. Petrov, and J. E. Greene, Phys. Rev. B **67**, 035409 (2003).
[30] S. F. Lin, D. T. Pierce, and W. E. Spicer, Phys. Rev. B **4**, 326 (1971).
[31] A $3\times3\times3$ array of unit cells with two atoms per unit cell in fcc symmetry (1 Pt and 1 N), results in 54 atoms (27 Pt and 27 N atoms). We removed 1 N atom to get $Pt_{27}N_{26}$.
[32] A $2\times2\times2$ array of unit cells with two atoms per unit cell in fcc (1 Pt and 1 N), results in 16 atoms (8 Pt and 8 N atoms). We removed 1 N atom to get Pt_8N_7.
[33] C. A. Fan, L. L. Sun, Y. X. Wang, Z. J. Wei, R. P. Liu, S. Y. Zeng, and W. K. Wang, Chin. Phys. Lett. **22**, 2637 (2005).